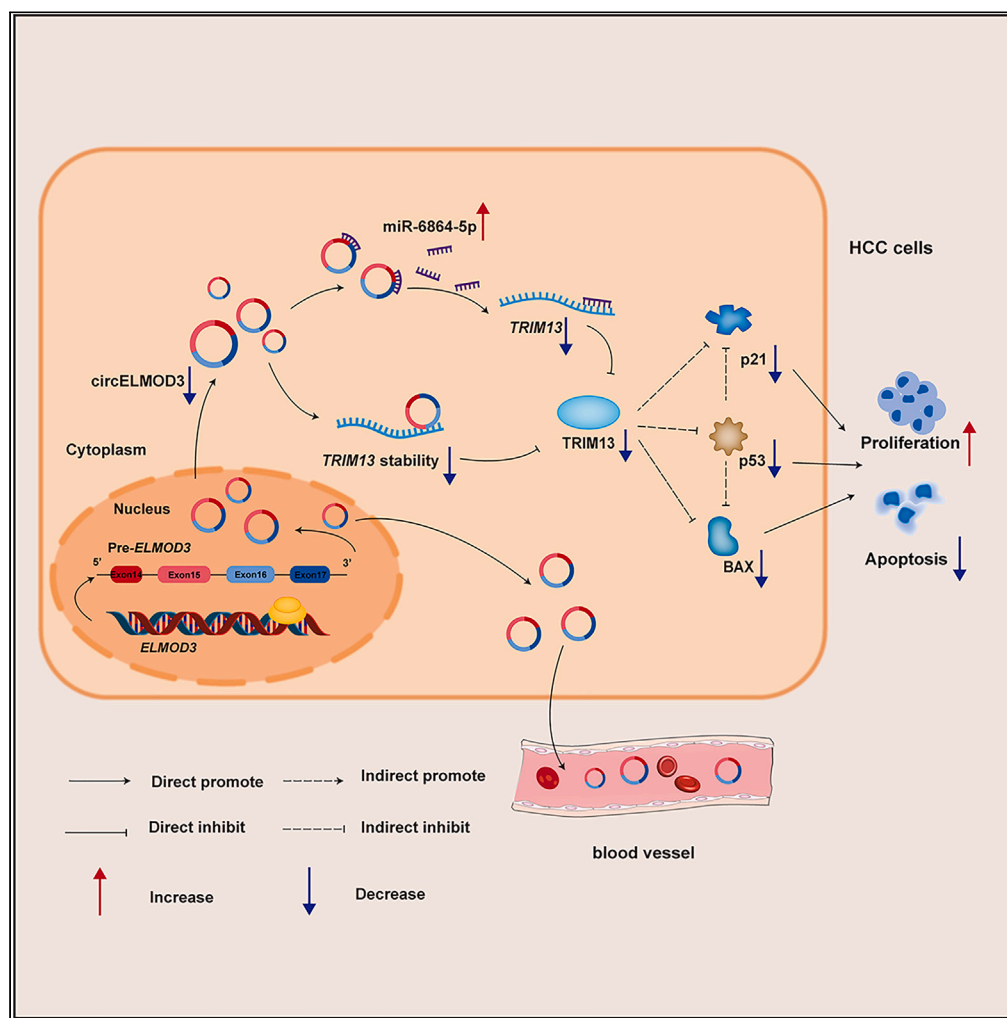**Article**

circELMOD3 increases and stabilizes *TRIM13* by sponging miR-6864-5p and direct binding to inhibit HCC progression

Mingshuang Lai,
Meiliang Liu,
Deyuan Li, ...,
Xiaogang Wang,
Aruo Nan, Xiaoyun
Zeng

nanaruo@163.com (A.N.)
zengxiaoyun@gxmu.edu.cn
(X.Z.)

Highlights
circELMOD3 was
significantly
downregulated in tissue
samples of HCC patients

circELMOD3 inhibited the
growth of HCC cells both *in
vitro* and *in vivo*

circELMOD3 increases
TRIM13 expression by
sponging miR-6864-5p
and direct binding

iScience

Article

circELMOD3 increases and stabilizes *TRIM13* by sponging miR-6864-5p and direct binding to inhibit HCC progression

Mingshuang Lai,[1,2,4] Meiliang Liu,[1,2,4] Deyuan Li,[1,2,4] Ruirui Zhang,[1,2] Lijun Wang,[1,2] Xiaofei Li,[1,2] Sixian Chen,[1,2] Siqian Wu,[1,2] Suyang Xiao,[1,2] Liling Wei,[1,2] Xiaogang Wang,[1,2] Aruo Nan,[1,2,*] and Xiaoyun Zeng[1,2,3,5,*]

SUMMARY

Many circular RNAs (circRNAs) have been identified to be associated with hepatocellular carcinoma (HCC) progression. We aim to explore the diagnostic potential, functions, and mechanism of circELMOD3 in HCC. Differentially expressed circRNAs in HCC and its paired adjacent tissues were identified by RNA sequencing. circELMOD3 was downregulated in HCC tissues and was related to clinicopathological characteristics of HCC patients. Additionally, plasma circELMOD3 was shown to be a highly sensitive and non-invasive biomarker to distinguish HCC from healthy controls. Functional assays showed that circELMOD3 inhibited proliferation and induced apoptosis of HCC cells both *in vitro* and *in vivo*. Mechanistically, RNA antisense purification (RAP) and luciferase reporter assays verified that circELMOD3 functioned as a sponge for miR-6864-5p leading to increased expression of its target gene *TRIM13*. Interestingly, RNA stability test demonstrated that circELMOD3 overexpression led to enhanced stability of its directly bound *TRIM13* mRNA, which in turn co-activated the p53 signaling pathway.

INTRODUCTION

Hepatocellular carcinoma (HCC) ranks the third leading cause of cancer-related death worldwide.[1] The onset of HCC is insidious and most patients are identified at advanced stages, which lead to a poor prognosis.[2] Early diagnosis and treatment is the primary strategy to improve the prognosis of HCC patients, and identification of non-invasive biomarkers is essential to the early detection of HCC.[3] Currently, alpha-fetoprotein (AFP) is the main circulating diagnostic biomarker for HCC, but it is not an ideal biomarker for early detection due to its relatively low sensitivity.[4] Thus, exploring new circulating biomarkers and in-depth investigation of the molecular mechanisms in the pathogenesis of HCC are of great significance to the better management of HCC patients.

Circular RNAs (circRNAs) belong to a newly discovered non-coding RNAs, characterized by structural stability and high conservation.[5] Numerous circRNAs have recently been identified as crucial regulators in tumor development.[6] Most circRNAs are abundant in tissues, cells, and body fluids, making them as ideal biomarkers.[7] For example, both hsa_circRNA_0039480 and hsa_circRNA_0026497 were elevated in the plasma of patients with gestational diabetes mellitus, and they may be used as diagnostic biomarkers.[8] Another circRNA, circSPARC, was increased in the plasma of colorectal cancer patients, and the receiver operating characteristic curve (ROC) analysis showed that circSPARC may be a candidate biomarker for patients with colorectal cancer.[9] In addition, accumulating evidence has revealed the potential diagnostic value of various circRNAs in many cancers.[10]

CircRNAs regulate tumor development through three key mechanisms: binding to key proteins,[11] acting as competitive endogenous RNA (ceRNA),[12] and translation of peptides,[13] of which the ceRNA mechanism is the most clearly clarified.[14] For instance, circKIF5B promotes HCC development through the adsorption of miR-192 and miR-215.[15] Similarly, hsa_circ_0003410 acts as a "molecular sponge" for miR-139-3p, thereby facilitating HCC progression.[16] In addition, circRNAs have also been shown to interact with specific mRNAs to affect their stability, which in turn regulates tumorigenesis and progression.[17–19] Previous studies on circRNAs mainly focused on the sponge effect of microRNAs (miRNAs). However, the regulation mechanisms may be diversified and whether they have multiple regulatory mechanisms to affect both the amount of mRNA expression as miRNA sponge and mRNA stability through direct binding remain to be clarified.

Considering the differential expression of circELMOD3 in HCC tissues, cell lines, and plasma, we hypothesized that circELMOD3 may participate in the pathogenesis of HCC. We aimed to investigate the biological function and the underlying mechanisms of circELMOD3 in the pathogenesis of HCC, as well as its potential as a diagnostic marker.

[1]School of Public Health, Guangxi Medical University, 22 Shuangyong Road, Nanning 530021, Guangxi, China
[2]Guangxi Colleges and Universities Key Laboratory of Prevention and Control of Highly Prevalent Diseases, Guangxi Medical University, Nanning 530021, Guangxi, China
[3]Key Laboratory of Early Prevention and Treatment for Regional High Frequency Tumor (Guangxi Medical University), Ministry of Education, Nanning, Guangxi, China
[4]These authors contributed equally
[5]Lead contact
*Correspondence: nanaruo@163.com (A.N.), zengxiaoyun@gxmu.edu.cn (X.Z.)
https://doi.org/10.1016/j.isci.2023.107818

RESULTS

circELMOD3 was notably downregulated in HCC tissues and cell lines

RNA-sequencing analysis showed that, a total of 94 circRNAs were differentially expressed in HCC tissues compared with adjacent normal tissues (Figure S1A). In order to further identify specific circRNA associated with HCC, we using log2|Fold Change|≥2.0 and adjusted p < 0.05 as cut-off, and 10 differentially expressed circRNAs were selected for further validation. Our results showed that circELMOD3 (circBase ID: hsa_circ_0004726) was the most downregulated circRNA in 30 pairs of mixed HCC tissue samples (Figure S1B), and this result was consistent with the sequencing data. Further validation in a larger cohort of tissue samples revealed that circELMOD3 was indeed down-regulated in 92 paired HCC tissue samples (Figure 1A). Subsequently, the expression of circELMOD3 was further examined in a panel of HCC cell lines with different metastatic properties, and we found that circELMOD3 expression levels in the three metastatic cell lines (MHCC97H, MHCC97L, and HCCLM3) were lower than those in the non-metastatic cell lines (Huh7, HepG2, and Hep3B) (Figure 1B). As the expression levels of circELMOD3 were down-regulated in both HCC tissues and cell lines, we selected circELMOD3 for further study.

We next moved on to verify the circular characteristics of circELMOD3 through several experiments. First, qPCR products amplified by circELMOD3-specific divergent primer were used for Sanger sequence analysis, thereby determining the head-to-tail splicing of circELMOD3 and the predicted splicing site (Figure 1C). Next, Hep3B and MHCC97H cells were treated with RNase R, and we found that circELMOD3 did not change in the presence of RNase R (Figures S1C and S1D). Third, we determined the half-life of circELMOD3 by applying actinomycin D, and found that circELMOD3 was more stable than linear *ELMOD3* mRNA (Figures 1D and 1E). Lastly, when the random primers and Oligo dT primers were used for qPCR, we found that the expression level of circELMOD3 was significantly lower compared to random primers, while the expression level of *ELMOD3* did not change (Figures 1F and 1G), indicating that circELMOD3 did not have a polyadenylate A tail. Collectively, these findings suggest that circELMOD3 is a stable circRNA molecule.

circELMOD3 was stably downregulated in the plasma of HCC patients and correlated with patient clinicopathological features

As circELMOD3 was abundant and notably downregulated in HCC tissues, we further explored whether circELMOD3 was expressed in plasma. We detected the expression levels of circELMOD3 in plasma of 150 HCC patients and 108 healthy controls, and found that circELMOD3 was significantly downregulated in HCC plasma (Figure S2A). ROC analysis showed that the sensitivity and specificity of circELMOD3 for detecting HCC were 81.50% and 85.30%, respectively, and the area under ROC curve (AUC) was 0.908 (Figure S2B). More-over, we used different storage conditions and repeated freeze-thaw experiments to test the stability of circELMOD3 in plasma of HCC patients and healthy controls. We found different storage conditions and repeated freezing and thawing processes had minimal effect on the expression levels of circELMOD3 (Figures S2C–S2F), implying that circELMOD3 is stable in human plasma.

To further explore the clinical significance of circELMOD3, we took the median expression of circELMOD3 as a cut-off value, and divided the study subjects into circELMOD3 low expression group and circELMOD3 high expression group. Then chi-square test was conducted to analyze the correlation between circELMOD3 expression and clinical characteristics/liver function index of HCC patients. The results of chi-square test showed that the expression levels of circELMOD3 was correlated with satellite nodules, tumor number, vascular invasion, lymphatic metastasis, AFP levels, and ki-67 positive rate of HCC patients (Table 1). In addition, downregulated circELMOD3 level was significantly associated with higher serum levels of total bilirubin (TBIL), aspartate aminotransferase (AST), and glutamate dehydrogenase (GDH) (Table S3). The results of the previous analysis suggest that the differential expression of circELMOD3 in HCC tissues has some clinical significance and may be associated with the prognosis of HCC patients.

circELMOD3 functioned as a tumor suppressor both *in vitro* and *in vivo*

To investigate the *in vitro* biological function of circELMOD3 in HCC, we used two siRNAs and plasmids to transiently silence or overexpress circELMOD3 in HCC cells (Figure S3A). When circELMOD3 was silenced or overexpressed, the expression of its parental gene *ELMOD3* was unaffected (Figure S3B). We then examined the effect of circELMOD3 on cellular behaviors. CCK-8 and EdU assays showed that cell proliferation was dramatically increased following circELMOD3 silencing, while these effects were abrogated upon circELMOD3 overexpression (Figures 2A–2C). Next, the impact of circELMOD3 on cell apoptosis was examined using a flow cytometry. As shown in Figures 2D and 2E, circELMOD3 silencing repressed cell apoptosis, whereas overexpression stimulated cell apoptosis. Results from transwell assays revealed that circELMOD3 silencing greatly facilitated cell migration and invasion, while overexpression showed the opposite results (Figures 2F–2H). All these data suggested that circELMOD3 functioned as a tumor suppressor *in vitro*.

To further explore the tumor suppressor role of circELMOD3 *in vivo*, we successfully constructed a MHCC97H cell line stably overexpressing circELMOD3 based on a lentivirus (LV) transfection system (Figure S3C). qPCR results demonstrated that the expression level of circELMOD3 was higher in LV-circELMOD3 group than it was in the negative control (NC) group (Figure S3D), while there was no statistically significance in the expression level of *ELMOD3* between the two groups (Figure S3E). Our *in vivo* study showed that tumor growth was much slower in the LV-circELMOD3 group than that in the LV-NC group (Figures 2I–2K). Immunohistochemistry analysis of removed tumors from nude mice showed the decreased levels of Ki-67, p53, BCL2 and the increased levels of BAX in the LV-circELMOD3 group compared to the LV-NC group, suggesting that the proliferation of HCC cells was suppressed while apoptosis was enhanced in the presence of circELMOD3 overexpression in nude mice model (Figure 2L).
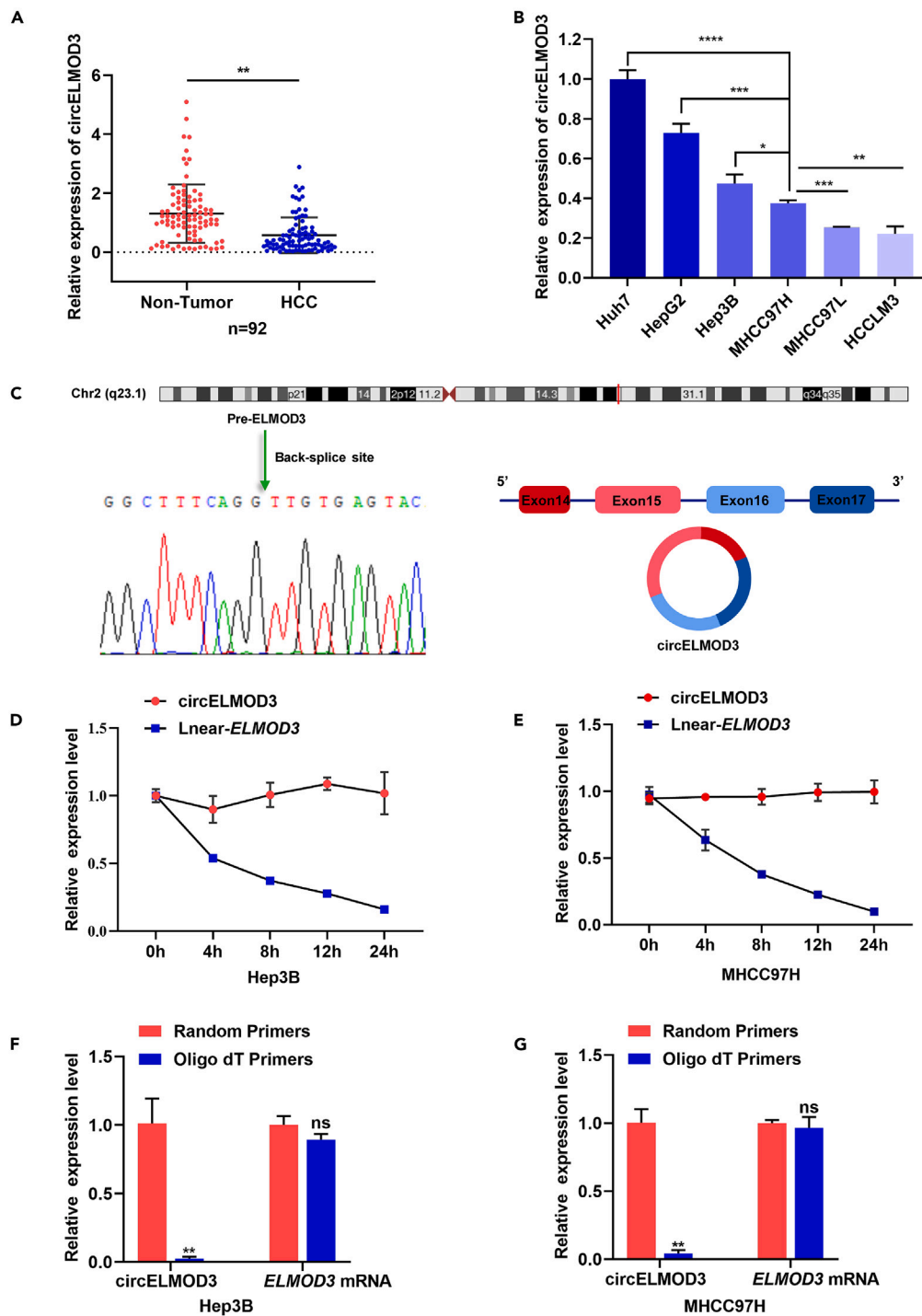
Figure 1. circELMOD3 was notably downregulated in HCC tissues and cell lines

(A) Relative expression of circELMOD3 in 92 pairs of HCC and adjacent normal tissue samples.

(B) Relative expression of circELMOD3 in six HCC cell lines.

(C) Sanger sequencing analysis of the qPCR product amplified by circELMOD3 divergent primer.

(D and E) qPCR analysis of the stability of circELMOD3 and *ELMOD3* in HCC cells treated with actinomycin D.

(F and G) Random primers and Oligo dT primers were used to conduct reverse transcription, and relative expression of circELMOD3 and *ELMOD3* were detected by qPCR. ns indicated no significance, *p < 0.05, **p < 0.01, ***p < 0.001, ****p < 0.0001. Data are represented as mean ± SD.

Table 1. Association between clinicopathological features and circELMOD3 in HCC patients

Variables	circELMOD3 expression		p value
	Low	High	
Age			
≤ 50	20	19	0.521
> 50	19	24	
Gender			
Female	3	7	0.235
Male	36	36	
HBsAg			
Positive	24	32	0.627
Negative	5	8	
Liver cirrhosis			
With	1	1	0.803
Without	28	40	
Satellite nodules			
Present	8	3	0.031*
Absent	23	38	
Tumor number			
Multiple	10	3	0.021*
Solitary	29	40	
Tumor size			
> 5cm	28	30	0.140
≤ 5cm	3	9	
Vascular invasion			
Present	11	2	0.004**
Absent	28	41	
Lymphatic metastasis			
Present	6	0	0.003**
Absent	25	41	
BCLC stage			
A	22	20	0.301
B + C	9	13	
AFP (ng/mL)			
≤ 400	10	23	0.024 *
> 400	15	10	
Ki-67 positive rate			
< 50%	15	29	0.009**
≥ 50%	15	7	

The expression level of circELMOD3 was examined by qPCR. Chi-squared test was employed to determine statistical difference. *$p < 0.05$, **$p < 0.01$.

circELMOD3 increased TRIM13 expression by sponging miR-6864-5p

We found that circELMOD3 was mainly distributed in the cytoplasm other than in the nucleus in HCC cells (Figure 3A), which was further confirmed by fluorescence *in situ* hybridization (FISH) assays (Figure 3B). Therefore, we explored whether circELMOD3 exerts its biological function in a ceRNA pattern. Through bioinformatics analysis (circBank, miRDB, circMine), we found 8 potential miRNAs that might bind to circELMOD3 (Figure 3C). RNA antisense purification (RAP) assays were performed to confirm the interactions between circELMOD3 and these candidate miRNAs (Figure 3D). Results from our studies suggested that the specific probe of circELMOD3 enriched circELMOD3 and seven candidate miRNAs except for miR-4716-3p (Figures 3E–3G). Among them, miR-6864-5p was the highest enriched miRNA. Accordingly, miR-6864-5p was chosen as one of the main target miRNAs of circELMOD3 for further analysis. Next, we detected the expression
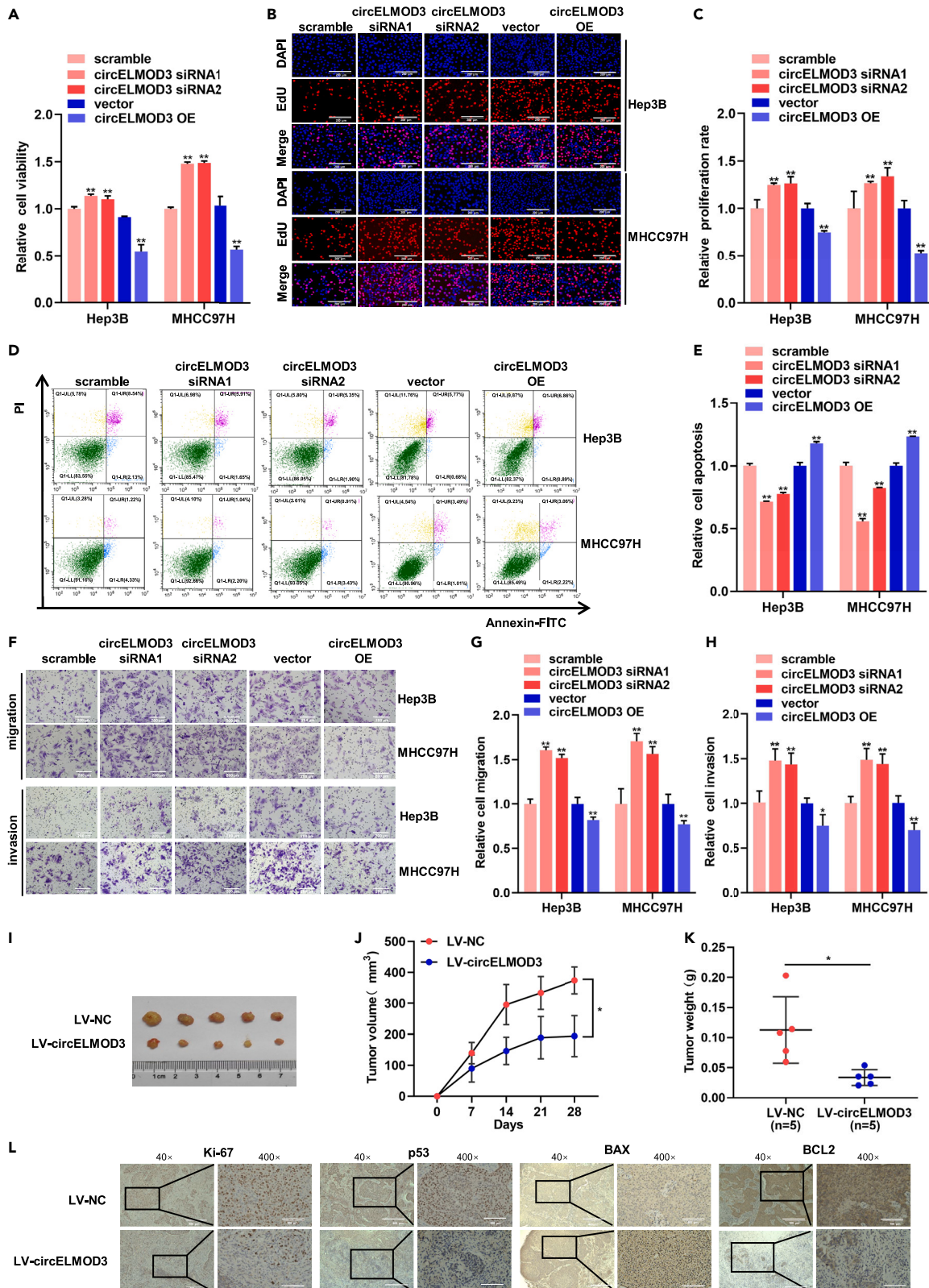
Figure 2. circELMOD3 functioned as a tumor suppressor both *in vitro* and *in vivo*

(A) CCK-8 assay was performed to detect cell viability when circELMOD3 was silenced or overexpressed in Hep3B and MHCC97H cell lines.

(B and C) EdU assay was used to detect cell proliferation when circELMOD3 was silenced or overexpressed in Hep3B and MHCC97H cell lines. Scale bar, 200 μm.

(D and E) Flow cytometry assay was used to measure cell apoptosis when circELMOD3 was silenced or overexpressed in Hep3B and MHCC97H cell lines.

(F–H) Transwell assays were used to detected cell migration and invasion when circELMOD3 was silenced or overexpressed in Hep3B and MHCC97H cell lines. Scale bar, 200 μm.

(I) MHCC97H cells stably overexpressing circELMOD3 (LV-circELMOD3) or negative control (LV-NC) were subcutaneous injection into the axilla of nude mice, and the tumors were removed after 28 days (n = 5 per group).

(J and K) Subcutaneous xenograft volume was measured in nude mice, and the weights were measured after the tumors were removed.

(L) Immunohistochemistry analysis of the expression levels of Ki-67, p53, BAX, and BCL2. ns indicated no significance, *p < 0.05, **p < 0.01, ***p < 0.001, ****p < 0.0001. Data are represented as mean ± SD.

pattern of miR-6864-5p when circELMOD3 was silenced or overexpressed in Hep3B and MHCC97H cells, and found that circELMOD3 could negatively regulate the expression of miR-6864-5p (Figure 3H). Simultaneously, we examined miR-6864-5p expression in HCC tissues and discovered that it was upregulated compared to adjacent tissues (Figure 3I). Further correlation analysis showed that the expression of circELMOD3 and miR-6864-5p were negatively correlated in HCC tissues (Figure 3J). To further verify the binding relationship between circELMOD3 and miR-6864-5p, the wild-type (WT) and mutant-type (MUT) of circELMOD3 luciferase reporter vectors were constructed (Figure 3K). And then the overexpression efficiency of miR-6864-5p mimic in HCC cells were determined (Figure S3F). Finally, dual luciferase reporter assays were conducted, and the results showed that miR-6864-5p mimic significantly attenuated the luciferase activity of circELMOD3-WT, but had no effect on the luciferase activity of circELMOD3-MUT compared to mimic NC (Figure 3L), confirming miR-6864-5p was able to bind circELMOD3.

Next, we used TargetScan, miRDIP, and miRWalk to predict the downstream target genes of miR-6864-5p. Combining binding capacity score, functional analysis and results from previous studies, 5 cancer-related genes were identified (Figure 4A). However, upon silencing or overexpression of circELMOD3, only *TRIM13* mRNA expression level was significantly downregulated or upregulated (Figures 4B and S4A–S4D). In addition, at the protein level, circELMOD3 could positively regulate the expression level of TRIM13 protein (Figures 4C and 4D). Besides, we detected the expression level of TRIM13 when miR-6864-5p was overexpressed in HCC cells, and the results showed that miR-6864-5p overexpression could decreased both the mRNA (Figure 4E) and protein (Figures 4F and 4G) levels of TRIM13. To further evaluate the relevance of these findings, we detected the expression of *TRIM13* in HCC tissues and found that it was downregulated compared to adjacent normal tissues (Figure 4H). Further correlation analysis showed that the expression of miR-6864-5p and *TRIM13* were inversely correlated in HCC tissues (Figure 4I). In addition, we also detected the expression levels of miR-6864-5p and *TRIM13* in our animal samples. The results showed that the expression level of miR-6864-5p was downregulated, while the expression level of *TRIM13* was upregulated when circELMOD3 was overexpressed in our animal model (Figures S4E and S4F). To further verify the interaction between miR-6864-5p and *TRIM13*, we performed bioinformatic analysis (http://rna.informatik.uni-freiburg.de/IntaRNA/Input.jsp) to see if there existed binding sequence between miR-6864-5p and *TRIM13*, and the results showed that *TRIM13* had a continuous binding sequence with miR-6864-5p (Figure 4J). Subsequently, *TRIM13*-WT and *TRIM13*-MUT luciferase reporter vectors were constructed (Figure 4K). As the results shown from dual luciferase reporter assays, *TRIM13*-WT's luciferase activity was decreased by miR-6864-5p-mimic, whereas *TRIM13*-MUT reversed this trend (Figure 4L), which validated the interaction between miR-6864-5p and *TRIM13*. Taken together, these data suggested that circELMOD3 upregulated the expression of *TRIM13* by sponging miR-6864-5p.

circELMOD3 directly binds to *TRIM13* mRNA and enhances its stability

Except for the ceRNA mechanism that circELMOD3 functions, we are also interested in whether circELMOD3 can bind to specific mRNA to exert its function. By bioinformatics analysis (http://rna.informatik.uni-freiburg.de/IntaRNA/Input.jsp), we found a contiguous binding site between circELMOD3 and *TRIM13* mRNA, and this suggested that circELMOD3 had the potential to interact with *TRIM13* mRNA (Figure 5A). Then we performed RAP assay to explore whether circELMOD3 and *TRIM13* mRNA could bind directly. Our results indicated that the specific probe of circELMOD3 enriched circELMOD3 and *TRIM13* mRNA notably (Figures 5B–5D). After confirming the binding relationship between circELMOD3 and *TRIM13* mRNA, we further explored whether circELMOD3 could influence the stability of *TRIM13* mRNA. We treated HCC cells with actinomycin D after silencing or overexpression of circELMOD3, and qPCR assays were performed to assess the stability of *TRIM13* mRNA. The results demonstrated that silencing circELMOD3 reduced (Figures 5E and 5F) while circELMOD3 overexpression increased (Figures 5G and 5H) the stability of *TRIM13* mRNA in HCC cells. Correlation analysis showed that the expression of circELMOD3 and *TRIM13* were positively correlated in HCC tissues (Figure 5I). Survival analysis from The Cancer Genome Atlas (TCGA) databases showed that patients with high *TRIM13* expression had longer overall survival (OS), disease-specific survival (DSS), and progression-free survival (PFS) compared to those with low *TRIM13* expression (Figure 5J). These results indicated that circELMOD3 stabilized *TRIM13* mRNA through direct binding and *TRIM13* might serve as a tumor suppressor in the progression of HCC.

circELMOD3 inhibits the progression of HCC through TRIM13/p53 axis

To investigate the underlying signaling pathway by which circELMOD3 participates, we detected the protein levels of NF-κB and p53 when circELMOD3 was silenced or overexpressed. Our results demonstrated that circELMOD3 stimulated p53 protein expression but had no effect
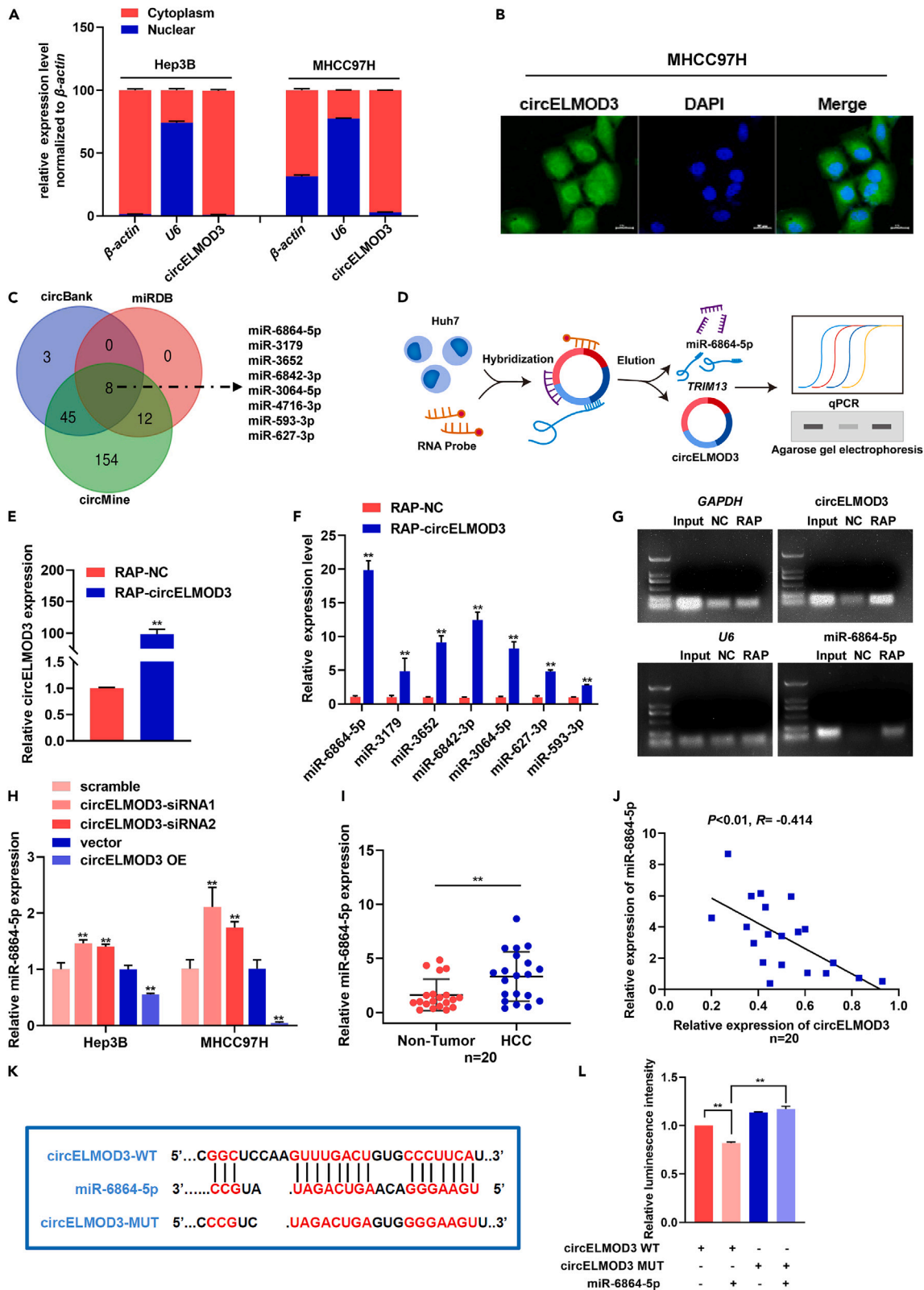
Figure 3. circELMOD3 functions as a sponge of miR-6864-5p

(A) Nucleoplasm separation analysis of cellular distribution of circELMOD3 in Hep3B and MHCC97H cell lines.

(B) FISH analysis of cellular localization of circELMOD3 in MHCC97H cell lines. Green indicates circELMOD3, nuclear were stained with DAPI. Scale bar, 20 μm.

(C) circBank, miRDB and circMine databases were used to predict circELMOD3-targeted miRNAs.

(D) Schematic diagram of the RAP experimental.

(E and F) After the RAP assay, relative expression levels of circELMOD3 and candidate miRNAs were detected by qPCR.

(G) After the RAP assay, DNA gel electrophoresis was performed on a 1% agarose gel.

(H) Relative expression of miR-6864-5p in circELMOD3 silenced and overexpressed HCC cells were detected by qPCR.

(I) Relative expression of miR-6864-5p in 20 pairs of HCC and adjacent normal tissue samples were detected by qPCR.

(J) Pearson correlation analysis of circELMOD3 expression and miR-6864-5p expression in tissue samples of 20 HCC patients.

(K) Diagram of *TRIM13* wild-type and mutant-type sequences.

(L) Dual luciferase reporter assay was used to verify the interaction between circELMOD3 and miR-6864-5p. ns indicated no significance, $*p < 0.05$, $**p < 0.01$, $***p < 0.001$, $****p < 0.0001$. Data are represented as mean ± SD.

on the protein levels of NF-κB (Figures 6A, 6C, S5A, and S5B). Based on these results, we hypothesized that circELMOD3 regulated HCC progression through p53-mediated biological signaling rather than the NF-κB pathway. We then performed pathway analysis of p53 through Kyoto encyclopedia of genes and genomes (KEGG), and found that p53 may regulate apoptosis and proliferation of HCC cells through regulating the expression of BAX and p21. In order to verify the hypothesis, we assessed the protein levels of BAX and p21 when circELMOD3 was silenced or overexpressed in MHCC97H cells, and the results demonstrated that circELMOD3 could positively regulate the expression of BAX and p21 (Figures 6B and 6C). We also examined the expression of BCL2, an anti-apoptosis protein, and found that overexpression of circELMOD3 could decrease the expression of BCL2, while silenced circELMOD3 abrogated this trend (Figures 6B and 6C). Additionally, we used HepG2 to further verify the downstream mechanism of circELMOD3. The results showed that the mRNA expression levels of *TRIM13*, *p53*, *p21*, and *BAX* were increased when circELMOD3 was overexpressed in HepG2 cells (Figures S5C–S5F). These findings demonstrated that circELMOD3 could regulate the apoptosis and proliferation of HCC cells through p53 mediated biological signaling.

Rescue experiments were conducted to further validate the circELMOD3/miR-6864-5p/*TRIM13* and circELMOD3/*TRIM13* axis, which constitutes a bidirectional regulatory axis participated in the progression of HCC. Firstly, we used two siRNAs to silence *TRIM13* expression (Figure S5G). Then we co-transfected circELMOD3 overexpression plasmid and miR-6864-mimic or *TRIM13* siRNA to conduct rescue experiments. Flow cytometry assays showed that both miR-6864-5p overexpression and *TRIM13* silencing could abolish the pro-apoptotic effect of circELMOD3 overexpression on HCC cells (Figures 6D and 6E). CCK-8 assays suggested that circELMOD3 overexpression inhibited cell viability, but these effects could be reversed by miR-6864-5p overexpression and *TRIM13* silencing (Figure 6F). EdU experiments indicated that both miR-6864-5p overexpression and *TRIM13* silencing could abrogate the anti-proliferation effect mediated by circELMOD3 overexpression (Figures 6G and 6H). Furthermore, western blot analysis demonstrated that *TRIM13* silencing could abolish the increased protein levels of p53, p21, and BAX induced by circELMOD3 overexpression, and reversed the decreased protein level of BCL2 induced by circELMOD3 overexpression (Figures 6I and 6J). In addition, immunohistochemical analysis of the tumors from nude mice revealed that TRIM13 was expressed at a higher level in the LV-circELMOD3 group than in the LV-NC group (Figure S5H). Collectively, results from our research indicated that circELMOD3 could not only increase the expression levels of *TRIM13* by sponging miR-6864-5p but also stabilize *TRIM13* mRNA through direct binding to inhibit the progression of HCC partly through p53-mediated biological signaling rather than the NF-κB pathway.

DISCUSSION

In recent years, numerous studies have reported the role of differentially expressed circRNAs in the pathogenesis of tumors.[20] By RNA sequencing, we identified that circELMOD3 was downregulated in HCC tissues and this trend was verified in HCC cell lines. As a circRNA confirmed by various methods, circELMOD3 was stable in plasma and was associated with clinicopathological features in HCC patients, which implying its potential as a non-invasive biomarker for HCC. Functional studies revealed that circELMOD3 inhibited proliferation and induced apoptosis of HCC cells both *in vitro* and *in vivo*. We further demonstrated that circELMOD3 increased and stabilized *TRIM13* expression by sponge adsorption of miR-6864-5p and direct binding leading to activation of the p53 signaling pathway to inhibit HCC progression.

CircRNAs in the blood are potentially useful as circulating biomarkers for HCC. For example, the AUC of serum circRNA_104075, and serum circ-FOXP1 for the early diagnosis of HCC were 0.932 and 0.973, respectively.[21,22] Our current study demonstrated that circELMOD3 was detectable, stable and downregulated in the plasma of HCC patients compared to healthy controls. Further ROC analysis showed that plasma circELMOD3 could be a promising circulating biomarker to distinguish HCC patients from healthy controls (AUC = 0.908).

Numerous dysregulated circRNAs in HCC tissues have been reported to exert vital biological functions in the pathogenesis and progression of HCC.[23] For example, hsa_circRNA_104348,[24] circRNA-100338,[25] and circCPSF6[26] have been shown to promote HCC progression, while cSMARCA5,[27] circRPN2,[28] and circDLC1[29] displayed a tumor suppressor role in HCC. Downregulated circELMOD3 in the HCC patient tissues was not reported before, so we focused on exploring the role of circELMOD3 in HCC and its underlying mechanisms in our current study. We first modulated the expression levels of circELMOD3 using siRNAs to silence or plasmid to overexpress in Hep3B and MHCC97H cells, and cell proliferation and apoptosis were evaluated. Overexpression of circELMOD3 suppressed proliferation, metastasis, and promoted apoptosis of HCC cells, while silencing circELMOD3 showed the opposite effect, which were further validated in the HCC nude mouse model. Data from our *in vitro* and *in vivo* studies confirmed the suppressor role of circELMOD3 in HCC.
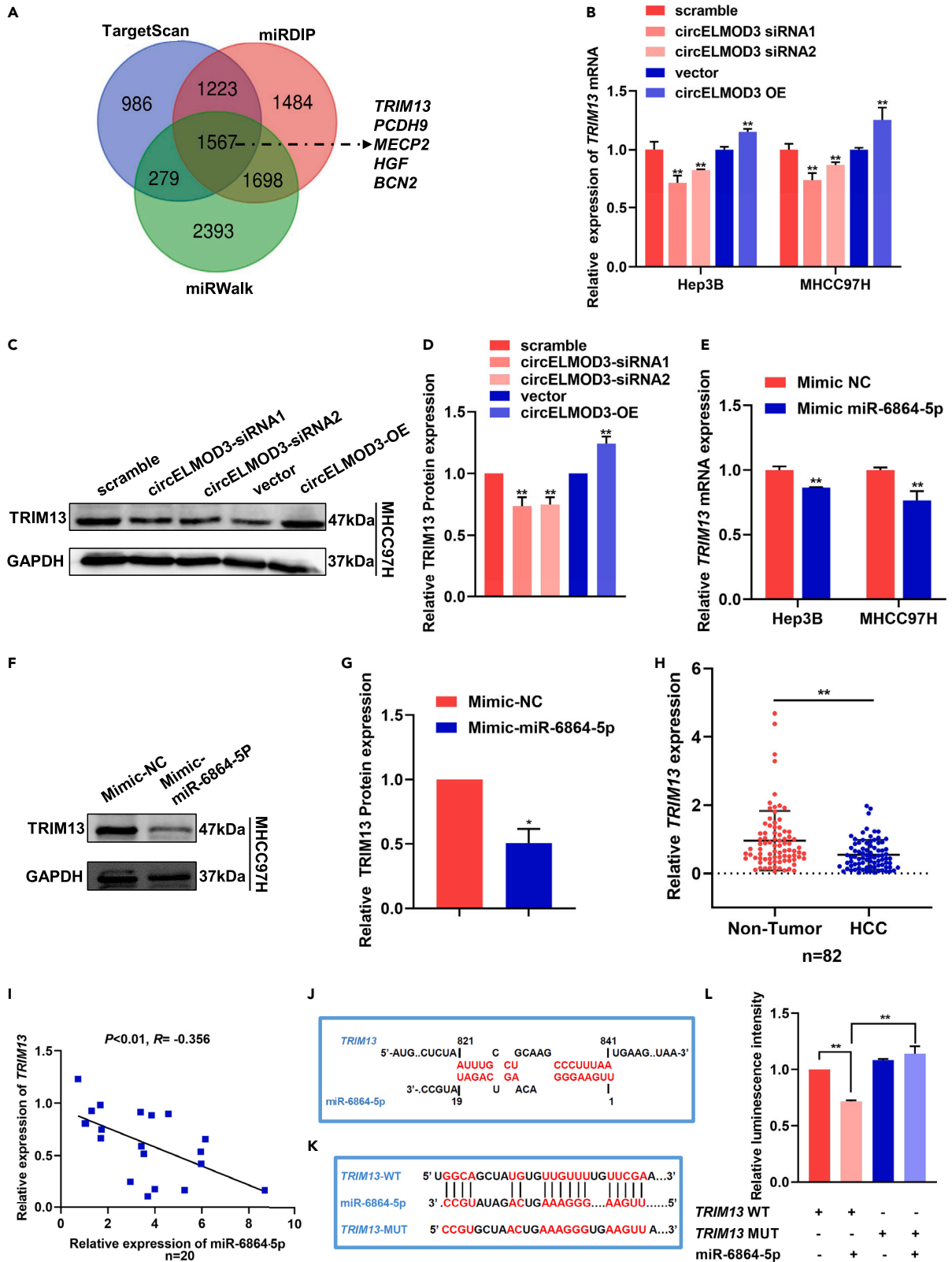
Figure 4. circELMOD3 increases *TRIM13* expression by sponging miR-6864-5p

(A) TargeScan, miRDIP and miRWalk databases were used to predict miR-6864-5p targeted mRNA.

(B) Relative expression of *TRIM13* mRNA in circELMOD3 silenced and overexpressed HCC cells.

(C and D) Relative protein level of TRIM13 in circELMOD3 silenced and overexpressed MHCC97H cells.

(E) Relative mRNA expression levels of *TRIM13* in miR-6864-5p overexpression cells.

(F and G) Relative protein levels of TRIM13 in miR-6864-5p overexpression cells.

(H) Relative expression of *TRIM13* in 82 pairs of HCC and adjacent normal tissue samples.

(I) Pearson correlation analysis of miR-6864-5p and *TRIM13* expression in tissue samples of 20 HCC patients.

(J) Bioinformatic analysis of binding sequencing between circELMOD3 and *TRIM13*. (K) Diagram of *TRIM13* wild-type and mutant-type sequences.

(L) Dual luciferase reporter assay was used to verify the interaction between miR-6864-5p and *TRIM13*. ns indicated no significance, *p < 0.05, **p < 0.01, ***p < 0.001, ****p < 0.0001. Data are represented as mean ± SD.

In order to explore the potential mechanisms on how circELMOD3 suppressed HCC, we first performed a subcellular localization assay. We found that circELMOD3 was mainly localized in the cytoplasm other than in the nucleus, which was further confirmed by FISH assays, indicating circELMOD3 may function as a sponge to specific miRNAs. Bioinformatics analysis identified 8 potential miRNAs that might bind to circELMOD3, which were confirmed by RAP interaction assays. Of the seven candidate miRNAs enriched by specific probe of circELMOD3, miR-6864-5p was the highest enriched miRNA. Therefore, miR-6884-5p was chosen as one of the main target miRNAs of circELMOD3 for further analysis. We found that circELMOD3 could negatively regulate the expression of miR-6864-5p in both Hep3B and MHCC97H cells as well as in HCC tissues. To further verify the binding relationship between circELMOD3 and miR-6864-5p, the WT and MUT of circELMOD3 luciferase reporter vectors were constructed. We found that miR-6864-5p mimic significantly attenuated the luciferase activity of circELMOD3-WT, but had no effect on the luciferase activity of circELMOD3-MUT compared to mimic NC, confirming miR-6864-5p was able to bind circELMOD3. Collectively, our data supported our findings that circELMOD3 sponged miR-6864-5p to negatively regulate the expression of miR-6864-5p. We then move forward to identify the target genes of miR-6864-5p and confirmed *TRIM13* as one of the main ones. We then detect the expression of *TRIM13* in our tissue samples and found that *TRIM13* was downregulated in HCC tissues. The downregulation of *TRIM13* in HCC tissues was consistent with the findings of previous reports on other cancer tissues.[30–32] Further validation in our animal samples showed that when circELMOD3 was overexpressed in our animal models, *TRIM13* was upregulated, while miR-6864-5p was down-regulated in tumor tissue samples of nude mice. Additional Pearson correlation analysis showed that the expression of miR-6864-5p and *TRIM13* were inversely correlated in HCC tissues. Taken together, these data suggested that circELMOD3 upregulated the expression of *TRIM13* by sponging miR-6864-5p. Data from our study also revealed that circELMOD3 stabilized *TRIM13* mRNA through direct binding. Francesca Rossi et al. reported that circZNF609 regulated tumorigenicity of rhabdomyosarcoma by interacting with *CKAP5* mRNA to affect its stability.[17] Similarly, circMET, may bind to *CDKN2A* mRNA and shorten the half-life of *CDKN2A* mRNA in renal cell carcinoma.[33] Another circRNA, circBRWD1 has been shown to bind directly to 3 mRNAs (*c-JUN*, *c-MYC*, *CDK6*), and affecting their stability in lung cancer.[18] Collectively, our findings demonstrated that circELMOD3 could increase and stabilize *TRIM13* expression in HCC.

TRIM13 belongs to the tripartite motif (TRIM) family and is a type of E3 ubiquitin-conjugating enzyme.[34] The TRIM family proteins are involved in a wide range of biological processes and play critical regulatory roles in the development of cancers.[35] Studies have shown that some TRIM proteins, including TRIM13,[36] TRIM24,[37] and TRIM28,[38] are involved in p53 regulation. It has been reported that TRIM13 mediated the ubiquitination and degradation of MDM2, leading to enhanced transcriptional activity and stability of p53.[36] Studies also confirmed that the endoplasmic reticulum resident TRIM13 protein stimulated NF-κB signaling by regulating the activation and translocation of its family members p65 and c-Rel. Silence of TRIM13 reduced the activation of p65, while the translocation of c-Rel into the nucleus was blunted.[39] TRIM13 interacts with tumor necrosis factor receptor-associated factor 6 (TRAF6) and potentiates NF-κB activity through ubiquitination of TRAF6.[40] Both NF-κB and p53 signaling pathways are important pathways that regulate tumor development. Therefore, we directly verify the role of circELMOD3 in these two signaling pathways. To verify this hypothesis, we conducted western blot assay to detect the protein levels of p53 and NF-κB in circELMOD3 silenced and overexpression MHCC97H cells. Surprisingly, we found that circELMOD3 could regulate the protein level of p53 rather than NF-κB. Next, we found through the KEGG pathway enrichment analysis that p53 could regulate the proliferation and apoptosis of HCC cells by regulating the expression of p21 and BAX. Previous studies showed that TRIM13 was increased by ionizing radiation in a dose- and time-dependent manner, TRIM13 overexpression induced cell death with increased expression of apoptotic molecules (p53, p21, and BAX).[36] To further investigate the downstream mechanism of circELMOD3 and p53, we detected the protein levels of p21 and BAX in circELMOD3 silenced and overexpressed MHCC97H cells, and the results showed that circELMOD3 could positively regulate the expression of these two proteins. Since Hep3B is a p53-deficient cell line, we used HepG2 to further verify the downstream mechanism of circELMOD3, and the results showed that the mRNA expression levels of *TRIM13*, *p53*, *p21*, and *BAX* were increased when circELMOD3 was overexpressed. These results indicated that circELMOD3 involved in p53 signaling pathway to inhibit HCC progression.

In summary, results from our research indicated that circELMOD3 could not only increase the expression levels of *TRIM13* by sponging miR-6864-5p but also stabilize *TRIM13* mRNA through direct binding to inhibit the progression of HCC partly through p53-mediated biological signaling pathway.

Limitation of the study

Firstly, we confirmed the interaction between circELMOD3 and *TRIM13* only by RAP assay, and it would be more convincing if the dual luciferase reporter assays could be conducted to further detect the interaction. Secondly, we only explored the downstream mechanisms
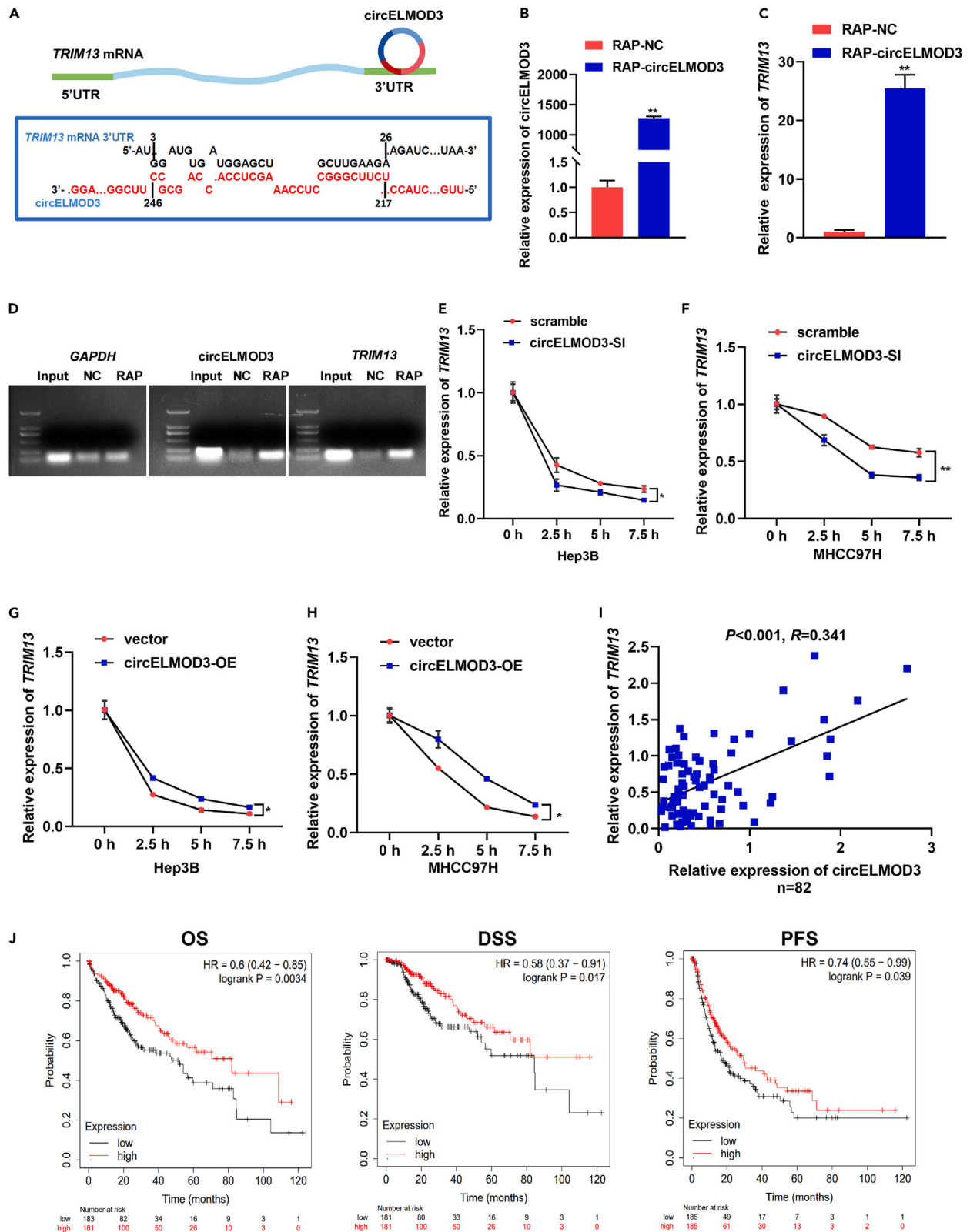
Figure 5. circELMOD3 directly binds to *TRIM13* mRNA and enhances its stability

(A) Schematic diagram of the binding sequence of circELMOD3 to *TRIM13* mRNA.

(B and C) After the RAP assay, relative expression levels of circELMOD3 and *TRIM13* mRNA were detected by qPCR.

(D) After the RAP assay, DNA gel electrophoresis was performed on a 1% agarose gel.

(E–H) Analysis of the stability of *TRIM13* mRNA after actinomycin D treatment.

(I) Pearson correlation analysis of circELMOD3 and *TRIM13* expression in tissue samples of 82 HCC patients.

(J) TCGA analysis of the association between *TRIM13* expression and prognosis of HCC patients. ns indicated no significance, *p < 0.05, **p < 0.01,***p < 0.001, ****p < 0.0001. Data are represented as mean $\pm$ SD.

of circELMOD3, and the underlying mechanism of circELMOD3 downregulation in HCC needs to be further studied. Thirdly, although plasma circELMOD3 deserved great diagnostic value for HCC patients in our studied sample, circELMOD3 was a downregulated circRNA, and the diagnostic value and clinical application of plasma circELMOD3 required prospective studies in a large cohort of patient samples.

STAR★METHODS

Detailed methods are provided in the online version of this paper and include the following:

- KEY RESOURCES TABLE
- RESOURCE AVAILABILITY
  - ○ Lead contact
  - ○ Materials availability
  - ○ Data and code availability
- EXPERIMENTAL MODELS AND SUBJECT DETAILS
  - ○ Tissues and plasma
  - ○ The role of circELMOD3 in the pathogenesis of HCC in nude mice model
  - ○ Cell culture
- METHOD DETAILS
  - ○ RNA sequencing
  - ○ Cell transfection
  - ○ RNA extraction, reverse transcription, and quantitative PCR (qPCR)
  - ○ Plasma RNA extraction and the stability test of circELMOD3 in plasma
  - ○ Verification of the circular structure of circELMOD3
  - ○ Cell proliferation and apoptosis assays
  - ○ Migration and invasion analysis
  - ○ Subcellular localization analysis of circELMOD3
  - ○ RAP assay
  - ○ Dual luciferase reporter assay
  - ○ RNA stability test
  - ○ Western blot analysis
  - ○ Survival analysis
- QUANTIFICATION AND STATISTICAL ANALYSIS

SUPPLEMENTAL INFORMATION

Supplemental information can be found online at https://doi.org/10.1016/j.isci.2023.107818.

AUTHOR CONTRIBUTIONS

Z.X.Y. and N.A.R. conceived of the study, L.M.S, L.M.L., and L.D.Y. performed the experiments, analyzed and wrote the paper. Z.R.R. and W.L.J. provided guidance for this work and revised the manuscripts and figures. L.X.F. and C.S.X. provide guidance for this work and responsible for manuscript submission. W.S.Q. and X.S.Y. was responsible for the bioinformatics analysis of the study. W.L.L. and W.X.G. collected the clinical samples and revised the manuscript. Z.X.Y. and N.A.R. revised the paper. The final manuscript was reviewed and approved by all authors.
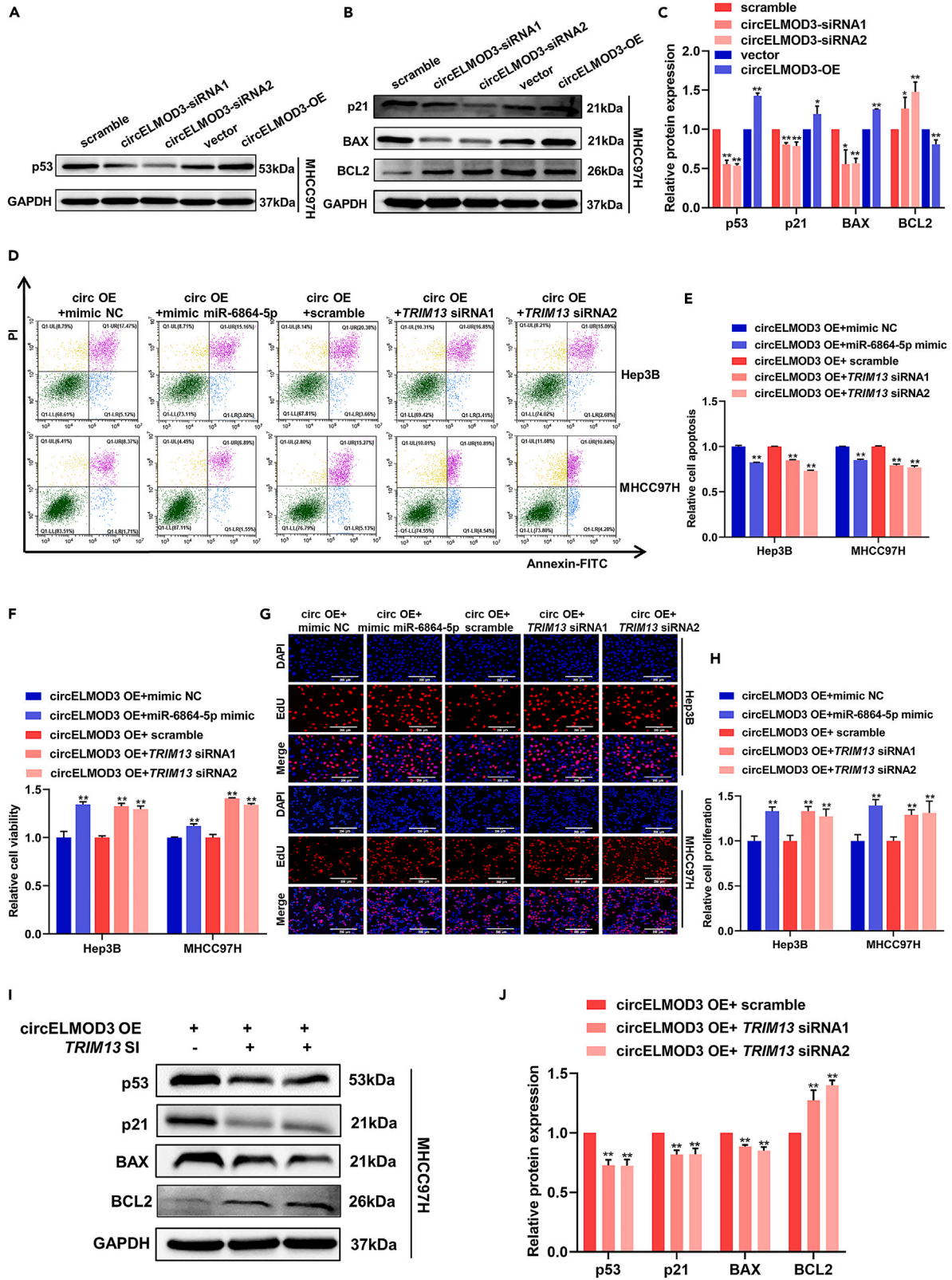
Figure 6. circELMOD3 inhibited the progression of HCC through TRIM13/p53 axis

(A–C) Protein levels of p53, p21, BAX and BCL2 when circELMOD3 was silenced or overexpressed in MHCC97H cells.

(D and E) Flow cytometry was used to detect cell apoptosis after co-transfected with circELMOD3 plasmid/vector and miR-6864-5p mimic/mimic NC or TRIM13 siRNAs/scramble.

(F) CCK-8 assays were used to detect cell viability after co-transfection.

(G and H) EdU assays were used to detect cell proliferation after co-transfection. Scale bar, 200 μm.

(I and J) Protein levels of p53, p21, BAX, and BCL2 were detected by western blot after co-transfection. ns indicated no significance, *p < 0.05, **p < 0.01, ***p < 0.001, ****p < 0.0001. Data are represented as mean ± SD.

DECLARATION OF INTERESTS

The authors declare no competing interests.

REFERENCES

1. Sung, H., Ferlay, J., Siegel, R.L., Laversanne, M., Soerjomataram, I., Jemal, A., and Bray, F. (2021). Global Cancer Statistics 2020: GLOBOCAN Estimates of Incidence and Mortality Worldwide for 36 Cancers in 185 Countries. CA. Cancer J. Clin. 71, 209–249. https://doi.org/10.3322/caac.21660.

2. Sun, J.Y., Zhang, X.Y., Cao, Y.Z., Zhou, X., Gu, J., and Mu, X.X. (2020). Diagnostic and prognostic value of circular RNAs in hepatocellular carcinoma. J. Cell Mol. Med. 24, 5438–5445. https://doi.org/10.1111/jcmm.15258.

3. Nault, J.C., and Villanueva, A. (2021). Biomarkers for Hepatobiliary Cancers. Hepatology 73 (Suppl 1), 115–127. https://doi.org/10.1002/hep.31175.

4. Harding-Theobald, E., Louissaint, J., Maraj, B., Cuaresma, E., Townsend, W., Mendiratta-Lala, M., Singal, A.G., Su, G.L., Lok, A.S., and Parikh, N.D. (2021). Systematic review: radiomics for the diagnosis and prognosis of hepatocellular carcinoma. Aliment. Pharmacol. Ther. 54, 890–901. https://doi.org/10.1111/apt.16563.

5. Shen, H., Liu, B., Xu, J., Zhang, B., Wang, Y., Shi, L., and Cai, X. (2021). Circular RNAs: characteristics, biogenesis, mechanisms and functions in liver cancer. J. Hematol. Oncol. 14, 134. https://doi.org/10.1186/s13045-021-01145-8.

6. Chen, L.L. (2020). The expanding regulatory mechanisms and cellular functions of circular RNAs. Nat. Rev. Mol. Cell Biol. 21, 475–490. https://doi.org/10.1038/s41580-020-0243-y.

7. Wen, G., Zhou, T., and Gu, W. (2021). The potential of using blood circular RNA as liquid biopsy biomarker for human diseases. Protein Cell 12, 911–946. https://doi.org/10.1007/s13238-020-00799-3.

8. Jiang, B., Zhang, J., Sun, X., Yang, C., Cheng, G., Xu, M., Li, S., and Wang, L. (2022). Circulating exosomal hsa_circRNA_0039480 is highly expressed in gestational diabetes mellitus and may be served as a biomarker for early diagnosis of GDM. J. Transl. Med. 20, 5. https://doi.org/10.1186/s12967-021-03195-5.

9. Wang, J., Zhang, Y., Song, H., Yin, H., Jiang, T., Xu, Y., Liu, L., Wang, H., Gao, H., Wang, R., and Song, J. (2021). The circular RNA circSPARC enhances the migration and proliferation of colorectal cancer by regulating the JAK/STAT pathway. Mol. Cancer 20, 81. https://doi.org/10.1186/s12943-021-01375-x.

10. Liao, W., Feng, Q., Liu, H., Du, J., Chen, X., and Zeng, Y. (2023). Circular RNAs in cholangiocarcinoma. Cancer Lett. 553, 215980. https://doi.org/10.1016/j.canlet.2022.215980.

11. Razpotnik, R., Vidmar, R., Fonović, M., Rozman, D., and Režen, T. (2022). Circular RNA hsa_circ_0062682 Binds to YBX1 and Promotes Oncogenesis in Hepatocellular Carcinoma. Cancers 14, 4524. https://doi.org/10.3390/cancers14184524.

12. Liu, Y., Song, J., Zhang, H., Liao, Z., Liu, F., Su, C., Wang, W., Han, M., Zhang, L., Zhu, H., et al. (2022). EIF4A3-induced circTOLLIP promotes the progression of hepatocellular carcinoma via the miR-516a-5p/PBX3/EMT pathway. J. Exp. Clin. Cancer Res. 41, 164. https://doi.org/10.1186/s13046-022-02378-2.

13. Duan, J.L., Chen, W., Xie, J.J., Zhang, M.L., Nie, R.C., Liang, H., Mei, J., Han, K., Xiang, Z.C., Wang, F.W., et al. (2022). A novel peptide encoded by N6-methyladenosine modified circMAP3K4 prevents apoptosis in hepatocellular carcinoma. Mol. Cancer 21, 93. https://doi.org/10.1186/s12943-022-01537-5.

14. Kristensen, L.S., Jakobsen, T., Hager, H., and Kjems, J. (2022). The emerging roles of circRNAs in cancer and oncology. Nat. Rev. Clin. Oncol. 19, 188–206. https://doi.org/10.1038/s41571-021-00585-y.

15. Fei, Z., Wang, Y., Gu, Y., Xie, R., Hao, Q., and Jiang, Y. (2022). CircKIF5B Promotes Hepatocellular Carcinoma Progression by Regulating the miR-192 Family/XIAP Axis. Front. Oncol. 12, 916246. https://doi.org/10.3389/fonc.2022.916246.

16. Cao, P., Ma, B., Sun, D., Zhang, W., Qiu, J., Qin, L., and Xue, X. (2022). hsa_circ_0003410 promotes hepatocellular carcinoma progression by increasing the ratio of M2/M1 macrophages through the miR-139-3p/CCL5 axis. Cancer Sci. 113, 634–647. https://doi.org/10.1111/cas.15238.

17. Rossi, F., Beltran, M., Damizia, M., Grelloni, C., Colantoni, A., Setti, A., Di Timoteo, G., Dattilo, D., Centrón-Broco, A., Nicoletti, C., et al. (2022). Circular RNA ZNF609/CKAP5 mRNA interaction regulates microtubule dynamics and tumorigenicity. Mol. Cell 82, 75–89.e9. https://doi.org/10.1016/j.molcel.2021.11.032.

18. Li, X., Chen, S., Wang, X., Zhang, R., Yang, J., Xu, H., He, W., Lai, M., Wu, S., and Nan, A. (2022). The pivotal regulatory factor circBRWD1 inhibits arsenic exposure-induced lung cancer occurrence by binding mRNA and regulating its stability. Mol. Ther. Oncolytics 26, 399–412. https://doi.org/10.1016/j.omto.2022.08.006.

19. Zhao, M., Wang, Y., Tan, F., Liu, L., Hou, X., Fan, C., Tang, L., Mo, Y., Wang, Y., Yan, Q., et al. (2022). Circular RNA circCCNB1 inhibits the migration and invasion of nasopharyngeal carcinoma through binding and stabilizing TJP1 mRNA. Sci. China Life Sci. 65, 2233–2247. https://doi.org/10.1007/s11427-021-2089-8.

20. Li, J., Sun, D., Pu, W., Wang, J., and Peng, Y. (2020). Circular RNAs in Cancer: Biogenesis, Function, and Clinical Significance. Trends Cancer 6, 319–336. https://doi.org/10.1016/j.trecan.2020.01.012.

21. Zhang, X., Xu, Y., Qian, Z., Zheng, W., Wu, Q., Chen, Y., Zhu, G., Liu, Y., Bian, Z., Xu, W., et al. (2018). circRNA_104075 stimulates YAP-dependent tumorigenesis through the regulation of HNF4a and may serve as a diagnostic marker in hepatocellular carcinoma. Cell Death Dis. 9, 1091. https://doi.org/10.1038/s41419-018-1132-6.

22. Wang, W., Li, Y., Li, X., Liu, B., Han, S., Li, X., Zhang, B., Li, J., and Sun, S. (2020). Circular RNA circ-FOXP1 induced by SOX9 promotes hepatocellular carcinoma progression via sponging miR-875-3p and miR-421. Biomed. Pharmacother. 121, 109517. https://doi.org/10.1016/j.biopha.2019.109517.

23. Louis, C., Leclerc, D., and Coulouarn, C. (2022). Emerging roles of circular RNAs in liver cancer. JHEP Rep. 4, 100413. https://doi.org/10.1016/j.jhepr.2021.100413.

24. Huang, G., Liang, M., Liu, H., Huang, J., Li, P., Wang, C., Zhang, Y., Lin, Y., and Jiang, X. (2020). circRNA hsa_circRNA_104348 promotes hepatocellular carcinoma progression through modulating miR-187-3p/RTKN2 axis and activating Wnt/β-catenin pathway. Cell Death Dis. 11, 1065. https://doi.org/10.1038/s41419-020-03276-1.

25. Huang, X.Y., Huang, Z.L., Huang, J., Xu, B., Huang, X.Y., Xu, Y.H., Zhou, J., and Tang, Z.Y. (2020). Exosomal circRNA-100338 promotes hepatocellular carcinoma metastasis via enhancing invasiveness and angiogenesis.

J. Exp. Clin. Cancer Res. *39*, 20. https://doi.org/10.1186/s13046-020-1529-9.

26. Chen, Y., Ling, Z., Cai, X., Xu, Y., Lv, Z., Man, D., Ge, J., Yu, C., Zhang, D., Zhang, Y., et al. (2022). Activation of YAP1 by N6-Methyladenosine-Modified circCPSF6 Drives Malignancy in Hepatocellular Carcinoma. Cancer Res. *82*, 599–614. https://doi.org/10.1158/0008-5472.Can-21-1628.

27. Yu, J., Xu, Q.G., Wang, Z.G., Yang, Y., Zhang, L., Ma, J.Z., Sun, S.H., Yang, F., and Zhou, W.P. (2018). Circular RNA cSMARCA5 inhibits growth and metastasis in hepatocellular carcinoma. J. Hepatol. *68*, 1214–1227. https://doi.org/10.1016/j.jhep.2018.01.012.

28. Li, J., Hu, Z.Q., Yu, S.Y., Mao, L., Zhou, Z.J., Wang, P.C., Gong, Y., Su, S., Zhou, J., Fan, J., et al. (2022). CircRPN2 Inhibits Aerobic Glycolysis and Metastasis in Hepatocellular Carcinoma. Cancer Res. *82*, 1055–1069. https://doi.org/10.1158/0008-5472.Can-21-1259.

29. Liu, H., Lan, T., Li, H., Xu, L., Chen, X., Liao, H., Chen, X., Du, J., Cai, Y., Wang, J., et al. (2021). Circular RNA circDLC1 inhibits MMP1-mediated liver cancer progression via interaction with HuR. Theranostics *11*, 1396–1411. https://doi.org/10.7150/thno.53227.

30. Xu, L., Wu, Q., Zhou, X., Wu, Q., and Fang, M. (2019). TRIM13 inhibited cell proliferation and induced cell apoptosis by regulating NF-κB pathway in non-small-cell lung carcinoma

cells. Gene *715*, 144015. https://doi.org/10.1016/j.gene.2019.144015.

31. Chen, W.X., Cheng, L., Xu, L.Y., Qian, Q., and Zhu, Y.L. (2019). Bioinformatics analysis of prognostic value of TRIM13 gene in breast cancer. Biosci. Rep. *39*. https://doi.org/10.1042/bsr20190285.

32. Li, H., Qu, L., Zhou, R., Wu, Y., Zhou, S., Zhang, Y., Cheng, B., Ni, J., Huang, H., and Hou, J. (2020). TRIM13 inhibits cell migration and invasion in clear-cell renal cell carcinoma. Nutr. Cancer *72*, 1115–1124. https://doi.org/10.1080/01635581.2019.1675721.

33. Yang, L., Chen, Y., Liu, N., Lu, Y., Ma, W., Yang, Z., Gan, W., and Li, D. (2022). CircMET promotes tumor proliferation by enhancing CDKN2A mRNA decay and upregulating SMAD3. Mol. Cancer *21*, 23. https://doi.org/10.1186/s12943-022-01497-w.

34. Li, X., Yu, Z., Fang, Q., Yang, M., Huang, J., Li, Z., Wang, J., and Chen, T. (2022). The transmembrane endoplasmic reticulum-associated E3 ubiquitin ligase TRIM13 restrains the pathogenic-DNA-triggered inflammatory response. Sci. Adv. *8*, eabh0496. https://doi.org/10.1126/sciadv.abh0496.

35. Hatakeyama, S. (2011). TRIM proteins and cancer. Nat. Rev. Cancer *11*, 792–804. https://doi.org/10.1038/nrc3139.

36. Joo, H.M., Kim, J.Y., Jeong, J.B., Seong, K.M., Nam, S.Y., Yang, K.H., Kim, C.S., Kim, H.S.,

Jeong, M., An, S., and Jin, Y.W. (2011). Ret finger protein 2 enhances ionizing radiation-induced apoptosis via degradation of AKT and MDM2. Eur. J. Cell Biol. *90*, 420–431. https://doi.org/10.1016/j.ejcb.2010.12.001.

37. Allton, K., Jain, A.K., Herz, H.M., Tsai, W.W., Jung, S.Y., Qin, J., Bergmann, A., Johnson, R.L., and Barton, M.C. (2009). Trim24 targets endogenous p53 for degradation. Proc. Natl. Acad. Sci. USA *106*, 11612–11616. https://doi.org/10.1073/pnas.0813177106.

38. Wang, C., Ivanov, A., Chen, L., Fredericks, W.J., Seto, E., Rauscher, F.J., 3rd, and Chen, J. (2005). MDM2 interaction with nuclear corepressor KAP1 contributes to p53 inactivation. Embo j *24*, 3279–3290. https://doi.org/10.1038/sj.emboj.7600791.

39. Hatchi, E.M., Poalas, K., Cordeiro, N., N'Debi, M., Gavard, J., and Bidère, N. (2014). Participation of the E3-ligase TRIM13 in NF-κB p65 activation and NFAT-dependent activation of c-Rel upon T-cell receptor engagement. Int. J. Biochem. Cell Biol. *54*, 217–222. https://doi.org/10.1016/j.biocel.2014.07.012.

40. Huang, B., and Baek, S.H. (2017). Trim13 Potentiates Toll-Like Receptor 2-Mediated Nuclear Factor κB Activation via K29-Linked Polyubiquitination of Tumor Necrosis Factor Receptor-Associated Factor 6. Mol. Pharmacol. *91*, 307–316. https://doi.org/10.1124/mol.116.106716.

STAR★METHODS

KEY RESOURCES TABLE

REAGENT or RESOURCE	SOURCE	IDENTIFIER
Antibodies		
Rabbit polyclonal Anti-TRIM13	Abcam	Cat # ab234847
Rabbit polyclonal Anti-p21	Boster	Cat # BM4382
Rabbit polyclonal Anti-BAX	Boster	Cat # BA0315-2
Rabbit polyclonal Anti-GAPDH	Affinity	Cat # AF7018; RRID: AB_2839420
Mouse monoclonal anti-p53	Santa Cruz	Cat # SC-126; RRID: AB_628082
Rabbit polyclonal Anti-BCL2	SAB	Cat # 48675-1
Mouse monoclonal anti- NF-κB	Santa Cruz	Cat # SC-8008; RRID: AB_628017
HRP-conjugated Affinipure Goat Anti-Mouse IgG(H+L)	Proteintech	Cat # SA00001-1; RRID: AB_2722565
HRP-conjugated Affinipure Goat Anti- Rabbit IgG(H+L)	Cell Signaling Technology	Cat # 7074S
Bacterial and virus strains		
circELMOD3 siRNA1 sense: GGCUUUCAGGUUGUGAGUATT	GenePharma	N/A
circELMOD3 siRNA1 antisense: UACUCACAACCUGAAAGCCTT	GenePharma	N/A
circELMOD3 siRNA2 sense: CUUUCAGGUUGUGAGUACATT	GenePharma	N/A
circELMOD3 siRNA2 antisense: UGUACUCACAACCUGAAAGTT	GenePharma	N/A
TRIM13 siRNA1 sense: CCCUACAGUUACUGACUAATT	GenePharma	N/A
TRIM13 siRNA1 antisense: UUAGUCAGUAACUGUAGGGTT	GenePharma	N/A
TRIM13 siRNA2 sense: GCAACAGAUGCAGGAGUUUTT	GenePharma	N/A
TRIM13 siRNA2 antisense: AAACUCCUGCAUCUGUUGCTT	GenePharma	N/A
Chemicals, peptides, and recombinant proteins		
Lipofectamine 3000	Invitrogen	Cat # L3000015
ribo-FECT™ CP transfection solution	RiboBio	Cat # C10511-05
Trizol	Invitrogen	Cat # 15596018
Trizol LS	Invitrogen	Cat # 10296028
RNase R	Epicentre	Cat # RNR07250
cell counting kit-8	Dojindo	Cat # CK04
Annexin VFITC/PI	Keygen Biotech	Cat # KGA107
nuclear and cytoplasmic separation kit	Invitrogen	Cat # AM1921
Pierce™ BCA protein assay Kit	Thermo Fisher Scientific	Cat # 23227
penicillin streptomycin	Gibco	Cat # 15140112
4% paraformaldehyde	Solarbio	Cat # P1110

Continued

REAGENT or RESOURCE	SOURCE	IDENTIFIER
cDNA probe diluent	Boster	Cat # AR0063
actinomycin D	sigma	Cat # SBR00013-1ML
MEM medium	Gibco	Cat # CP21110161839
fetal bovine serum	Gibco	Cat # 10099141C
DMEM medium	Gibco	Cat # CP21110161839
Critical commercial assays		
GoScript Reverse Transcription System	Promega	Cat # A5002
GoTaq® qPCR Master Mix	Promega	Cat # A6001
Cell-Light EdUApollo567 In Vitro Kit	RiboBio	Cat # C10310-1
RAP kit	Bersin Bio	Cat # Bes5103
Dual Luciferase Reporter Assay System	Promega	Cat # E1910
Deposited data		
RNA sequencing datasets	This paper	GSE216115
Experimental models: Cell lines		
293T	Cell Bank of Shanghai Academy of Chinese Sciences	N/A
Hep3B	Cell bank of the Chinese academy of sciences	N/A
MHCC97H	CellCook Biotech Co. Ltd.	N/A
Huh7	Cell bank of the Chinese academy of sciences	N/A
HepG2	Cell bank of the Chinese academy of sciences	N/A
HCCLM3	Zhongshan Hospital, Fudan University of Shanghai	N/A
MHCC97L	CellCook Biotech Co. Ltd.	N/A
Experimental models: Organisms/strains		
BALB/c nude mice	Guangxi Medical University's Animal Experiment Center	N/A
Oligonucleotides		
PCR primer for qPCR experiments used in this work, see Table S1	This paper	N/A
circELMOD3 FISH probe: TGCCGCTCAAGTGGAAACCATGAACTTGG TTGATTT	Sangon Biotech	N/A
circELMOD3 RAP probe-1: CTTGGGCTC TGACCACCTCTGTACTCACAACCTGAAA GCCCAGGTCCTCCCAGTGGTTTC	Sangon Biotech	N/A
circELMOD3 RAP probe-2 TTGGGCTC TGACCACCTCTGTACTCACAACCTGA AAGCCCAGGTCCTCCCAGTGGTTT	Sangon Biotech	N/A
circELMOD3 RAP probe-3 TTGGGCTC TGACCACCTCTGTACTCACAACCTG AAAGCCCAGGTCCTCCCAGTGGT	Sangon Biotech	N/A
Software and algorithms		
ImageJ	NIH	N/A
GraphPad Prism 8	GraphPad	N/A
SPSS 26.0	IBM	N/A

RESOURCE AVAILABILITY

Lead contact

Further information and requests for resources and reagents should be directed to and will be fulfilled by the lead contact, Xiaoyun Zeng (zengxiaoyun@gxmu.edu.cn).

Materials availability

The study did not generate new unique reagents.

Data and code availability

- The RNA sequencing datasets used in this study have been publicly available deposited in the GEO database GSE216115.
- This paper does not report original code.
- Any additional information required to reanalyze the data reported in this paper is available from the lead contact upon request.

EXPERIMENTAL MODELS AND SUBJECT DETAILS

Tissues and plasma

92 paired HCC and adjacent normal tissues were collected from the Affiliated Cancer Hospital of Guangxi Medical University from 2018 to 2022. Plasma samples were collected from 150 HCC patients and 108 healthy controls in the Affiliated Cancer Hospital of Guangxi Medical University and the Physical Examination Department, of the First Affiliated Hospital of Guangxi Medical University from 2021 to 2022, respectively. The inclusion criteria of the patients: (1) Any new cases of HCC confirmed by pathological biopsy. (2) Patients who have not previously undergone radiotherapy or chemotherapy. The exclusion criteria of the patients: (1) Patients with coexisting other tumors. (2) Patients who have received preoperative radiotherapy or chemotherapy. Age and gender-matched healthy controls were selected from routine medical examination population and those with a previous or current history of tumor were excluded. The informed consent was acquired from each patient and the study was approved by the Ethics Committee of Guangxi Medical University. All methods were carried out in accordance with the Declaration of Helsinki.

The role of circELMOD3 in the pathogenesis of HCC in nude mice model

Male nude mice (BALB/c) aged 4-6 weeks were used for *in vivo* study. The experiment was divided into circELMOD3 overexpression group (LV-circELMOD3) and negative control group (LV-NC). Approximately 2×10^6 MHCC97H cells stably overexpressing circELMOD3 and control cells were administered to the right axilla of nude mice. The tumor volume was measured with vernier calipers every 3 days. After 28 days, the nude mice were sacrificed, and the solid tumors were excised and measured. Tumor volume $(mm^3)=length \times (width)^2/2$. The dissected tumors were processed for immunohistochemical analysis (Servicebio, China). The animal study was approved by the Animal Care &Welfare Committee of Guangxi Medical University. All methods were performed in accordance with relevant guidelines and regulations. This study was carried out in accordance with the ARRIVE guidelines.

Cell culture

The background information for the human HCC cell lines routinely maintained in our laboratory was described in the key resources table. Hep3B cells were cultured in MEM medium (Gibco, Carlsbad, CA, USA, CP21110161839) supplemented with 10% fetal bovine serum (FBS, Gibco, Carlsbad, CA, USA, 10099141C) and 1% penicillin streptomycin (PS, Gibco, Carlsbad, CA, USA, 15140112). HepG2, Huh7, MHCC97H, MHCC97L, HCCLM3, and 293T cells were cultured in DMEM medium (Gibco, Carlsbad, CA, USA, CP21110161839) supplemented with 10% FBS and 1% PS. All cells were incubated at 37°C incubator containing 5% CO_2. Each cell line was tested for mycoplasma before the experiments.

METHOD DETAILS

RNA sequencing

RNA sequencing was performed on 5 pairs of HCC and adjacent tissue samples by Lc-Bio Technologies (Hangzhou, China). Total RNA was isolated and purified from tissue samples. The RNA integrity was assessed by Agilent 2100 with RIN number>7.0. Approximately 5 μg of total RNA was used to remove ribosomal RNA according to the manuscript of the Ribo-Zero™ rRNA Removal Kit (Illumina, San Diego, USA). The cleaved RNA fragments were reverse-transcribed to produce cDNA. Finally, the paired-end sequencing was performed on an Illumina Hiseq 4000 (LC Bio, China) following the vendor's recommended protocol.

For bioinformatic analysis, Cutadapt was firstly used to remove the reads that contained adaptor contamination, low quality bases and undetermined bases. Then FastQC (http://www.bioinformatics.babraham.ac.uk/projects/fastqc/) was used to verified the sequence quality. Bowtie2 and Hisat2 were used to map reads to the genome of species. CIRCExplorer2 and CIRI were used to denovo assemble the mapped reads to circRNAs; Then, back splicing reads were identified in unmapped reads by tophat-fusion. $log2|Fold Change| \geq 2.0$ and adjusted $P<0.05$ of circRNAs between the two groups were considered differentially expressed.

Cell transfection

The overexpressed plasmid of circELMOD3 was constructed using pcDNA3.1 (Hunan Fenghui Biotechnology Co., Ltd). Plasmid extraction was performed using a plasmid midi kit (Qiagen, Germany, 12145) and transfection using Lipofectamine 3000 (Invitrogen, USA, L3000015). Briefly, 96- and 6-well plate were planted with 6×10^3 and 3×10^5 cells/well, respectively, and cultured for 18 h. Subsequently, 0.1 and 2.5 μg of plasmids were respectively employed to 96- and 6-well plate, and cultured for 48 h to complete the transfection process.

The expression of circELMOD3 and *TRIM13* was transiently silenced by two specific small interference RNA (siRNA), which were generated by GenePharma (Shanghai, China). Both siRNAs and miRNA mimics were transfected with ribo-FECT™ CP transfection solution (RiboBio, China, C10511-05). Briefly, 96- and 6-well plate were planted with 5×10^3 and 2×10^5 cells/well, respectively, and cultured for 18 h. Subsequently, 100 nM siRNAs and 50 nM miRNA mimics were respectively employed to 96- and 6-well plate, and cultured for 48 h to complete the transfection process.

The lentivirus vector containing circELMOD3 and a negative control were generated by GenePharma (Shanghai, China). MHCC97H cells were selected to construct circELMOD3 stably overexpressing cell lines through lentiviral transfection. After 72 h of lentivirus infection, we used puromycin (Solarbio, China, P8230) to screen successfully transfected MHCC97H cells. The transfection efficiency of overexpression and silence was verified by qPCR. Follow-up experiments were performed after confirming the specific silencing and overexpression efficiencies. All siRNA sequences were displayed in Table S1.

RNA extraction, reverse transcription, and quantitative PCR (qPCR)

Trizol reagent (Invitrogen, USA, 15596018) was used for extracting total RNA from cell lines and tissue samples. All extracted RNAs were quantified with Nano Drop one (Thermo Scientific, USA). Mir-X™ First Strand Synthesis Kit was used for miRNA reverse transcription (Takara, Japan, 638315). GoScript Reverse Transcription System was used to reverse transcription of circRNA and mRNA (Promega, USA, A5002). GoTaq® qPCR (Promega, USA, A6001) and Quant Studio™ 7 Flex Real-Time PCR (Applied Biosystem, USA) were used for all quantitative polymerase chain reactions (qPCR). *U6* was utilized as the internal reference of miRNA, while *β-actin* and *GAPDH* were used as the internal reference of circRNA and mRNA, respectively. The relative gene expression. was calculated by $2^{-\Delta\Delta CT}$ algorithm. All qPCR primers in this study were synthesized by Sangon Biotech and the sequences were displayed in Table S2.

Plasma RNA extraction and the stability test of circELMOD3 in plasma

Plasma RNA was extracted using Trizol LS (Invitrogen, USA, 10296028). The stability of circELMOD3 in plasma was evaluated by different storage conditions and repeated freeze-thaw experiments. Briefly, equal amounts of plasma were stored at room temperature, 4°C, and -80°C, and incubated for 0, 6, 12, 24, and 48 h. For repeated freeze-thaw experiments, equal amounts of plasma were repeatedly frozen/thawed for 0, 2, 4, and 6 times. The CT value of circELMOD3 in different conditions were detected by qPCR.

Verification of the circular structure of circELMOD3

The circular structure of circELMOD3 was verified through Sanger sequencing, linear RNA digestion enzymes (RNase R), and reverse transcription of Oligo dT primer and Random primer. Briefly, circELMOD3 qPCR products were sequenced by Sangon Biotech Co., Ltd. For RNase R treatment, 0.15 μL of 3 U/μg RNase R (Epicentre, USA, RNR07250) was incubated with 1μg of RNA at 37°C for 10 min. Subsequently, reverse transcription of RNase-treated and untreated RNA was performed. To further verify circELMOD3 did not have a polyadenylate A tail, reverse transcription was carried out by using an Oligo dT primer and a random primer, respectively. Finally, the expression levels of circELMOD3 and *ELMOD3* were detected by qPCR.

Cell proliferation and apoptosis assays

Cell proliferation was assessed using cell counting kit-8 (CCK-8, Dojindo, Japan, CK04) and The Cell-Light EdU Apollo567 In Vitro Kit (RiboBio, Guangzhou, China, C10310-1). Briefly, about 6×10^3 cells were seeded in each well of the 96-well plates, and transfected for 48 h. For the CCK-8 assay, 100 μL of fresh medium containing 10 μL of CCK-8 solution was added to the cells. Finally, the absorbance at 450 nm was measured after incubation at 37°C for 1.5 h. For the Edu assay, the Edu reagent was diluted with complete medium at 1:1000 and added to the cells, then incubated overnight following the manufacturer's instructions. An EVOS microscope (Thermo Scientific, USA) was used to capture images of the cells. The cell proliferative rate was calculated using Image J software.

Cell apoptosis was measured with Annexin VFITC/PI (Keygen Biotech, China, KGA107). Briefly, transfected cells were digested by trypsin EDTA-free (Solarbio, China, T1350), and resuspended with 350 μL of binding buffer. Then the cells were added with 5 μL of Annexin-FITC and PI reagent successively, and incubated in dark box for 15 min and 5 min respectively. The cells were finally added with 150 μL of binding buffer before flow cytometry detection (Beckman Coulter, USA).

Migration and invasion analysis

Cell migration and invasive ability were evaluated using the Transwell (Corning, USA, 3422). For the migration experiment, 700 μL of medium containing 10% FBS was added to the lower chamber and placed in the incubator for equilibration. About 5×10^4 cells were suspended in serum-free medium and seeded in the upper chamber. After culturing for 36 h, the cells in the chamber were washed twice with PBS, fixed with ethanol for 15 min, and then stained with crystal violet for 30 min. Cells on the upper membrane were wiped with a cotton swab. Images of

the stained cells were captured using a microscope. The method of the invasion experiment was the same as that of the migration experiment, except that the membrane of the Transwell was covered with Matrigel.

Subcellular localization analysis of circELMOD3

The subcellular localization of circELMOD3 was analyzed by nuclear and cytoplasmic separation (Invitrogen, USA, AM1921) followed by FISH assay. For the nuclear and cytoplasmic separation assay, about 1×10^6 cells were collected and the distribution ratio of circELMOD3 in the nucleus and cytoplasm was determined by qPCR. *U6* was used as nuclear control, and *β-actin* as cytoplasmic control. For FISH assay, coverslips were seeded with 5×10^4 MHCC97H cells and cultured for 36 h. The cells were fixed with 4% paraformaldehyde (Solarbio, China, P1110) for 1 h, and then underwent gradient dehydrated with 70%, 80%, 95% and 100% ethanol for 5 min, respectively. After denaturation at 78°C for 8 min, the FISH probe was diluted with cDNA probe diluent (BOSTER, China, AR0063). The probe was then added to the cells, and incubated at 42°C overnight in the dark. The next day, the cells were stained with DAPI for 10 min. Finally, the subcellular location of circELMOD3 was observed using an LSM800 confocal microscope (Zeiss, German). The FISH probe sequence of circELMOD3 was displayed in Table S1.

RAP assay

RAP experiments were performed using a RAP kit (Bersin Bio, China, Bes5103). Huh7 cells were cultured in 8 petri dish and cultured for 18 h. Subsequently, 5 μg of circELMOD3 overexpression plasmid was used to transfect cells. 24 h after transfection, cells were collected and cross-linked in PBS with 40 mL of 1% formaldehyde for 10 min, and 4 mL of 1.375 M glycine was added to neutralize the crosslinking reaction for 5 min. Then, the RAP group was hybridized with denaturation probe on a vertical mixer at room temperature for 1 h, while the NC group was not hybridized with probe. circELMOD3 and its interacting RNAs were captured by streptavidin magnetic beads (Bersin Bio, Bes5103-1). For RNA purification, 125 μL of phenol-chloroform-isoamyl alcohol mixture was added to each sample. After centrifugation and collection of the aqueous phase, 5 μL NaCl, 1 μL Glycogen, and 312.5 μL anhydrous ethanol were added and then precipitated at -80°C for 16 h. Finally, miR-NAs and *TRIM13* mRNA enriched in circELMOD3 conjugates were analyzed by qPCR and agarose gel electrophoresis. The RAP probes sequences were displayed in Table S1.

Dual luciferase reporter assay

The dual luciferase vectors of circELMOD3 and *TRIM13* were constructed (Hunan Fenghui Biotechnology Co., Ltd), and the Dual Luciferase Reporter Assay System was used to detect the luciferase activity (Promega, WI, USA, E1901). About 3.5×10^5 293T cells were seeded in 6-well plate and co-transfected with wild-type (WT) or mutant-type (MUT) plasmids, and miR-6864-5p mimics or mimic NC. 36 h after co-transfection, cells were collected and lysed with 1×passive lysis buffer. Then 100 μL of the luciferase assay reagent II was added to each well of the 96-well plate. The absorbance at 580 nm was by a microplate reader. Absorbance at 460 nm was measured after 100 μL of stop & Glo® reagent was added to the same well, the absorbance at 460 nm was measured. Firefly fluorescence was used to normalize Renilla fluorescence.

RNA stability test

About 2.5×10^5 cells were seeded in 6-well plate and transfected with circELMOD3 siRNA or plasmid, respectively. After transfection for 36 h, the cells were treated with 0.8 μg/μL actinomycin D (Sigma, Germany, SBR00013-1ML), and incubated at 37°C. Then total RNAs were collected at 0, 2.5, 5, and 7.5 h, respectively. Finally, the stability of RNA was determined by qPCR.

Western blot analysis

Proteins were extracted using a Lysis buffer (10 mM Tris-HCl, pH 7.4, 1% SDS, and 1 mM Na_3VO_4) and quantified by Pierce™ BCA assay (Thermo Fisher Scientific, USA, 23227). The proteins were isolated by an SDS-PAGE gel and electroblotted onto a polyvinylidene fluoride (PVDF) membrane (Bio-Rad, USA, 1620177). The PVDF membrane was first sealed with 5% skim milk at room temperature for 1 h, then incubated with the primary antibody in a shaker at 4°C overnight. The primary antibodies used in this study included Abcam (TRIM13, ab234847, 1:1000), SANTA GRUZ (p53, SC-126, 1:500; NF-κB SC-8008, 1:500), BSTER (p21, BM4382, 1:1000; BAX, BA0315-2, 1:500), SAB (BCL2, #48675-1, 1:500), and Affinity (GAPDH, AF7018, 1:5000). The secondary antibodies, including Cell Signaling Technology (anti-rabbit, 7074S, 1:5000) and Proteintech (Anti-Mouse, SA00001-1, 1:5000) were then incubated with the membranes at room temperature for 1 h. Finally, the ClinxS6 system (CLINX, China) was used for chemiluminescent imaging of the membrane. Grayscale analysis of protein bands was performed using Image J technology.

Survival analysis

The LIHC dataset of the TCGA database (https://cancergenome.nih.gov) was used to gather RNA sequencing data and the clinical information of HCC patients. We transformed the RNA expression data into the base-2 logarithm using the transcripts per million (TPM) unit of measurement. Then the correlation between *TRIM13* mRNA expression and the OS, DSS, and PFS in patients with liver cancer was determined, and the corresponding survival curves were obtained.

QUANTIFICATION AND STATISTICAL ANALYSIS

Statistical analysis of the experimental data was performed using SPSS software (version 26.0) and GraphPad Prism (version 8.0). The chi-square test and the un-paired t-test was applied to compare two sets of counting variables and continuous variables, respectively. The difference in circELMOD3 expression between HCC and adjacent normal tissue samples was compared using a paired t-test. The median value of circELMOD3 expression was calculated by SPSS. Using median expression as a cut-off value, the study subjects were divided into circELMOD3 low expression group and circELMOD3 high expression group. Then chi-square test was conducted to analyze the correlation between circELMOD3 expression and clinical characteristics/liver function index of HCC patients. The diagnostic efficacy of plasma circELMOD3 was evaluated using ROC. The correlation between the two quantitative variables was ascertained using Pearson correlation analysis. $p < 0.05$ was considered statistically significant. ns indicated no significance, $*p < 0.05$, $**p < 0.01$, $***p < 0.001$, $****p < 0.0001$. Data are represented as mean $\pm$ SD.